VTT PUBLICATIONS 551

Josephson junctions in charge and phase picture
Theory and applications

Juha Hassel

VTT Information Technology

Dissertation for the degree of Doctor of Science in Technology to be presented with due permission of the Department of Engineering Physics and Mathematics for public examination and debate in Large Seminar Hall of Micronova at Helsinki University of Technology (Espoo, Finland) on the 9th of November, 2004, at 12 o'clock noon.

ISBN 951–38–6418–9 (soft back ed.)
ISSN 1235–0621 (soft back ed.)

ISBN 951–38–6419–7 (URL: http://www.vtt.fi/inf/pdf/)
ISSN 1455–0849 (URL: http://www.vtt.fi/inf/pdf/)

JULKAISIJA – UTGIVARE – PUBLISHER

VTT, Vuorimiehentie 5, PL 2000, 02044 VTT
puh. vaihde (09) 4561, faksi (09) 456 4374

VTT, Bergsmansvägen 5, PB 2000, 02044 VTT
tel. växel (09) 4561, fax (09) 456 4374

VTT Technical Research Centre of Finland, Vuorimiehentie 5, P.O.Box 2000, FIN–02044 VTT, Finland
phone internat. + 358 9 4561, fax + 358 9 456 4374

VTT Tietotekniikka, Tietotie 3, PL 1207, 02044 VTT
puh. vaihde (09) 4561, faksi (09) 456 7012

VTT Informationsteknik, Datavägen 3, PB 1207, 02044 VTT
tel. växel (09) 4561, fax (09) 456 7012

VTT Information Technology, Tietotie 3, P.O.Box 1207, FIN–02044 VTT, Finland
phone internat. + 358 9 4561, fax + 358 9 456 7012

Technical editing Maini Manninen

Otamedia Oy, Espoo 2004

Hassel, Juha. Josephson junctions in charge and phase picture. Theory and applications. Espoo 2004. VTT Publications 551. 38 p. + app. 40 p.

Keywords Josephson junctions, quantum metrology, mesoscopic tunnel junctions

Abstract

Properties of weak links between two superconductors, or Josephson junctions, make them interesting for fundamental physics research. Since their discovery over four decades ago, they have provided a unique way to study the behavior of the superconducting quantum phase. More recently, ultra small, or mesoscopic, Josephson junctions with substantial single Cooper pair charging energy have gained interest due to their behavior as macroscopic quantum objects.

In addition to the theoretical interest, Josephson junctions can be used as active elements in circuit applications. Particularly, in this Thesis we study two different devices. We develop the required theoretical treatments, derive device properties, and compare the results with experimental data.

The first application is a Josephson voltage standard based on externally damped Superconductor - Insulator - Superconductor junctions. It consists of an array of large Josephson junctions connected in series and irradiated with a 70 GHz microwave signal. Phase locking the Josephson dynamics into the signal leads to the quantization of the voltage. This is utilized in metrology. We introduce a new circuit solution based on frequency dependent damping of the junctions. Optimization and some designs for practical arrays are presented. The purpose is to find such a design that the array is fast, has low power consumption and is as stable as possible. Arrays able to generate DC voltages of order 1 volt with metrological accuracy are demonstrated experimentally and their applicability in AC voltage calibrations is analyzed.

The second application is the Bloch Oscillating Transistor (BOT). The BOT is based on controlling the Cooper pair current in an ultra small Josephson junction by means of quasiparticles tunneling through a normal junction. As part of the thesis work, the principle of operation is first demonstrated computationally. The model is then refined to yield quantitative predictions of the characteristics. Finally, an analytic theory for the device is developed and the properties as an amplifier are derived.

Preface

The research work has been done as a part of the research projects in the Quantronics group and its predecessors at VTT Information Technology and VTT Automation over a time span of about five years. The work has been done in close collaboration with the co-workers. The collaboration with the Low Temperature Laboratory of Helsinki University of Technology, the VTT Microelectronics Centre and the Centre for Metrology and Accreditation (MIKES) has been especially valuable.

First of all, I wish to thank my instructor Prof. Heikki Seppä, whose inexhaustible ideas are mostly behind the work reported here. I also would like to thank the manager of the Quantronics group, Dr. Panu Helistö, whose advice and encouragement has been invaluable. Furthermore, I wish to thank my supervisor, Prof. Pekka Hautojärvi, who has been very helpful about organizing the things with the university.

I have also grately benefited from the help and discussions with our group members, Mikko Kiviranta, Arttu Luukanen, Antti Niskanen, Jari Penttilä, Hannu Sipola and Antti Virtanen. Also all the people working in the Microsensing research field have shown to be very helpful and entertaining to work with. I would especially like to thank Kaisa Falenius, Aija Kaski, Seija Lepistö, Elisa Pylvänäinen and Mia Sarvi for keeping the things running.

The contribution of our collaborators has been very important. The work of Leif Grönberg, Ilkka Suni and Markku Ylilammi in the JVS fabrication has been irreplacable. Jaani Nissilä's, Antti Kemppinen's and Kari Ojasalo's work at MIKES on further development of the JVS setup has also been of crucial value. Experimentalists at the Low Temperature Laboratory, Julien Delahaye, Rene Lindell, Mika Sillanpää, Prof. Pertti Hakonen and Prof. Mikko Paalanen, have made a crucial part of the work related to the BOT.

Finally, I would like to thank my parents for the support during the years.

List of publications

This Thesis is based on the following original publications:

Josephson voltage standard

P1. Hassel, J., Seppä, H., Grönberg, L. and Suni, I. 2001. SIS Junctions with Frequency Dependent Damping for a Programmable Josephson Voltage Standard. IEEE Trans. Instrum. Meas Vol. 50, No. 2, pp. 195–198.

P2. Hassel, J., Seppä, H., Grönberg, L. and Suni, I. 2003. Optimization of a Josephson Voltage Array Based on Frequency Dependently Damped Superconductor - Insulator - Superconductor Junctions. Rev. Sci. Instrum. Vol. 74, No. 7, pp. 3510–3515.

P3. Hassel, J., Grönberg, L., Helistö, P, Seppä, H., Nissilä, J. and Kemppinen, A. 2004. Fast Josephson Arrays for Voltage and Impedance Metrology. Conference of Precision Electromagnetic Measurements. London, 27 June – 2 July 2004, Conference Digest, pp. 154–155.

Bloch oscillating transistor

P4. Hassel, J. and Seppä, H. 2001. Analysis of the Bloch Oscillating Transistor. IEEE Trans. Appl. Supercond. Vol. 11, No. 1, pp. 260–262.

P5. Delahaye, J, Hassel, J., Lindell, Sillanpää R., Paalanen, M. Seppä. H. and Hakonen, P. 2003. Low-Noise Current Amplifier Based On Mesoscopic Josephson Junction. Science, Vol. 299, pp. 1045–1048.

P6. Hassel, J. Seppä, H., Delahaye, J. and Hakonen, P. 2004. Control of Coulomb Blockade in a Mesoscopic Josephson Junction Using Single Electron Tunneling. J. Appl. Phys. Vol. 95, No. 12, pp. 8059–8062.

P7. Hassel, J. and Seppä. H. Theory of the Bloch Oscillating Transistor. Submitted for publication.

The author's own contribution

In publications P1–P3 I did most of the modelling and design work for the devices as well as carried out most of the low-temperature experiments. In publications P4–P7 I took part in testing the ideas about the new device as well as largely did the simulations and the theoretical work to characterize its properties. Publications P1–P4 and P6–P7 are to a large part written by myself. I also participated in the writing process of publication P5.

Table of contents

1. Introduction

Brian Josephson showed theoretically in 1962 that two weakly coupled superconductors can exhibit peculiar phenomena related to Cooper pairs tunneling through the link [1]. He predicted that with a constant voltage V applied across such a link, which was later named Josephson junction (JJ), the current through the junction oscillates with frequency $2eV/h$. He also predicted that a current can flow through the junction without a voltage drop, if the current is smaller than a "critical current". These effects are manifestations of the dynamics of the quantum phase difference Φ across the junction.

Since then, theoretical, experimental and technological understanding on Josephson phenomena and their applications has increased substantially. Especially the development of reliable fabrication techniques has made it possible to create applications for a variety of purposes. These include sensors for magnetic fields, amplifiers, passive and active components for RF and millimeter wave technology, etc. (for an overview see e.g. [2]).

More recently, a new class of phenomena was discovered in small junctions, in which the charging energy of a single charge carrier (a Cooper pair) is comparable to other energy scales in the system [3, 4]. This includes the blockade of charge flow at small voltages (the Coulomb blockade) as well as novel coherent charge oscillations called the Bloch oscillations.

In this Thesis, we first give a brief review of the physics of Josephson junctions starting from the phenomenological description as a single quantum object. Models in the limit of large and mesoscopic junctions are derived. Then they are applied to the devices under study. Finally, theoretical and experimental results from the devices are presented.

2. Physics of Josephson junctions

A. General

The Josephson junction is a macroscopic quantum object described by Hamiltonian [3]

$$H = \frac{Q^2}{2C} - \left(\frac{\Phi_0}{2\pi} I(t)\,\Phi + E_J \cos(\Phi) \right) + H_q, \tag{1}$$

where the first term is the capacitive charging energy, second term is the interaction with an external current source $I(t)$, third term is the Josephson coupling and fourth term is the interaction with the quasiparticle system and the electromagnetic environment. Here Q is the charge operator, C is the junction capacitance, and E_J is the Josephson coupling energy. The superconducting flux quantum is $\Phi_0 = h/2e \approx 2.07 \times 10^{-15}$ Vs. A schematic circuit diagram of a JJ is shown in Fig. 1(a). The cross symbolizes Josephson coupling, the capacitor the capacitive coupling and $\overline{Z}(\omega)$ the electromagnetic environment. The current $I(t)$ is also shown.

The operators for charge Q and phase Φ satisfy the following commutation relation:

$$[\Phi, Q] = 2ei, \tag{2}$$

i.e. they are bound by the Heisenberg uncertainty relation. The charge operator can be written in terms of phase as

$$Q = \frac{2e}{i} \frac{\partial}{\partial \Phi}. \tag{3}$$

From Eqs. (1)-(3) one can draw an analogy to a particle moving in a sinusoidal potential shown in Fig. 1(b). Mathematically this "washboard potential" $U(\Phi, t)$ is given as

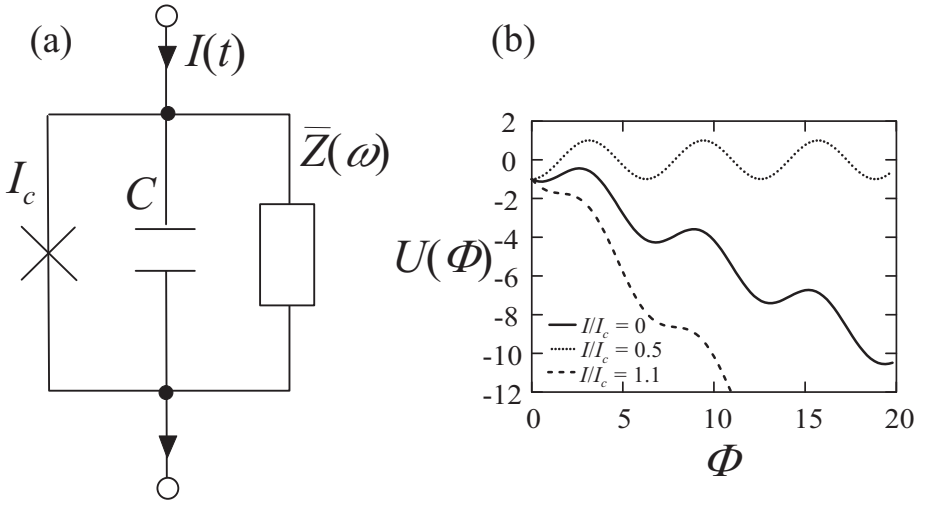

Figure 1. (a) The circuit diagram of a Josephson junction connected parallel to an impedance $\overline{Z}(\omega)$. (b) Washboard potential $U(\Phi)$ as function of the quantum phase difference Φ.

$$U(\Phi,t) = -E_J\left(\frac{I(t)}{I_c}\Phi + \cos\Phi\right), \tag{4}$$

where I_c is the critical current of the junction. The position of the "particle" corresponds to phase difference Φ, and momentum to charge Q. Tilting of the potential depends on $I(t)$, while the amplitude of the "bumps" is E_J. The dissipation of the particle is included in H_q. The Josephson coupling energy is related to the critical current as

$$E_J = \frac{\Phi_0 I_c}{2\pi}. \tag{5}$$

B. Large Josephson junctions

Here we consider the limit, where both the phase Φ and the charge Q are assumed to be classical variables. This is the case, if the quantum energies $\hbar\omega$ of all frequencies ω present in the system are small compared to E_J and the thermal energy k_BT as explained below [5]. Assuming the Hamiltonian in Eq. (1) to be classical and solving the equations of motion $\partial H/\partial Q = (\Phi_0/2\pi)(\partial\Phi/\partial t)$ and $(2\pi/\Phi_0)(\partial H/\partial\Phi) = -\partial Q/\partial t$ one obtains

$$V = \frac{\Phi_0}{2\pi}\frac{\partial\Phi}{\partial t} \tag{6}$$

$$I(t) = C\frac{\partial V}{\partial t} + I_S(t) + I_c\sin\Phi, \tag{7}$$

where we have defined voltage across the junction $V = Q/C$ and marked $I_S(t) = \partial H_q/\partial\Phi$ ("the shunt current"). The displacement current due to junction capacitance is the first term on the right hand side of Eq. (7). The quasiparticle tunnel current as well as the current through circuit elements connected parallel to the junction ($\overline{Z}(\omega)$ in Fig. 1) are accounted for by the second term. In case of externally damped junctions (see Section III), the quasiparticle tunnel current is usually small and it thus can be neglected. If the circuit connected parallel to the junction is linear, I_S is obtained from the linear circuit theory. In general, it includes both a deterministic part and a fluctuation associated with the real part of $\overline{Z}(\omega)$. The Cooper pair tunnel current through the JJ is the third term.

In the simplest case the junction is damped with a linear resistor, i.e. $Z(\omega) = R$, and thus $I_S = V/R + I_n$, where I_n is a random variable, whose spectral density satisfies the Nyquist formula $\langle I_n^2\rangle = 4kT/R$ [6]. Then Eqs. (6) and (7) can be written as

$$\beta_c\frac{d^2\Phi}{d\tau^2} + \frac{d\Phi}{d\tau} + \sin\Phi = i(\tau) + i_n(\tau). \tag{8}$$

This is called the resistively and capacitively shunted junction (RCSJ) model for a Josephson junction. Here the dimensionless time $\tau = (2\pi I_cR/\Phi_0)t$ and the dimensionless current $i(\tau) = I(t)/I_c$. The hysteresis parameter is defined as $\beta_c = \left(2\pi I_cR^2C\right)/\Phi_0$.

To study the range of the applicability of the model, we will first note that an important characteristic frequency of a junction is the plasma frequency f_p, i.e. the frequency of the oscillation within a minimum in the washboard potential. From the circuit picture of Fig. 1(a) this can also be interpreted as the L_JC oscillation in the junction capacitance and the Josephson inductance L_J. For small bias currents and phase variations the linearized tunnel element behaves as an inductance $L_J = \Phi_0/2\pi I_c$. The angular plasma frequency $\omega_p = 1/\sqrt{L_JC}$ can then be written as

$$\omega_p = \sqrt{\frac{2\pi}{\Phi_0}\frac{I_c}{C}}. \tag{9}$$

Using the definition of E_J in Eq. (5) and defining the single electron charging energy

$$E_C = \frac{e^2}{2C}, \tag{10}$$

the energy levels of the plasma oscillation can be written as

$$E_p = \hbar\omega_p\left(N + \frac{1}{2}\right) = \sqrt{8E_JE_C}\left(N + \frac{1}{2}\right) \tag{11}$$

with N as an integer. A sufficient requirement for the classical approximation to hold is that the spacing of the levels $\Delta E_p = \sqrt{8E_JE_c}$ is small compared to E_J and k_BT i.e.

$$\frac{E_J}{E_C} \gg 8 \tag{12}$$

$$\frac{(kT)^2}{E_CE_J} \gg 8. \tag{13}$$

Typical tunnel junction fabrication techniques (see e.g. Section III) produce junctions with critical current densities J_c above 10^5 A/m^2 and specific capacitance $C_s \approx 0.05$ F/m^2. For junctions having dimensions above 1 μm this leads to $E_J/E_C \gtrsim 100$. If measurements are performed at the liquid helium temperature, $T = 4.2$ K, then $(k_BT)^2/E_CE_J \gtrsim 400$.

In principle, also other frequencies present at the system (driving signals, characteristic frequencies of the system consisting of the junction and the rest of the circuit) should be studied to prove the applicability of the model. However, these are typically not substantially above f_p. Thus the treatment above is sufficient to state that devices fabricated with optical litography and measured at liquid He can be handled classically. As the temperature is lowered, it is sometimes necessary to apply quantum corrections, especially if the fluctuations of the system are studied [7].

C. Ultrasmall junctions

With electron beam litography one can fabricate junctions having lateral dimensions from 10 nm to 100 nm. In this case the condition of Eq. (12) fails. With cooling techniques such as dilution

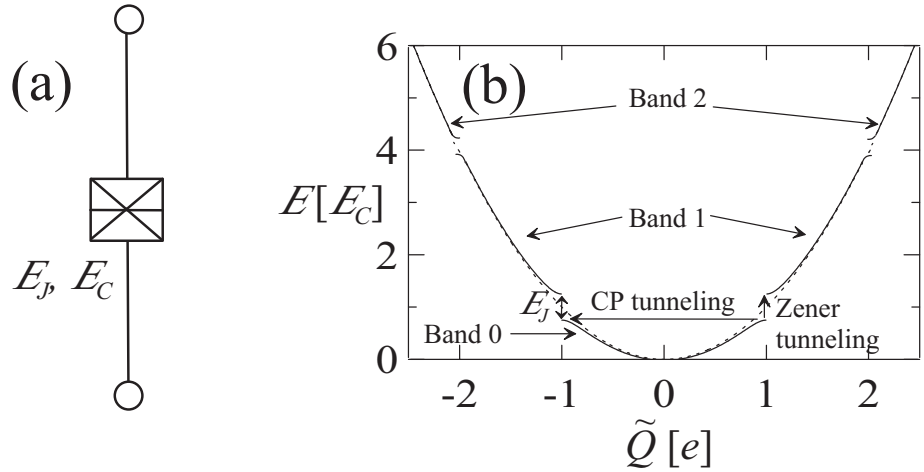

Figure 2. (a) The drawing symbol of a mesoscopic Josephson junction and (b) the band diagram in the "weak binding limit". Possible transitions, i.e. Cooper pair tunneling and Zener tunneling, are indicated with arrows.

refrigeration or adiabatic demagnetization, temperatures below 100 mK can be reached. In this case also the condition of Eq. (13) fails.

To understand the dynamics of ultra small junctions, we will again start from the Hamiltonian in Eq. (1), but assume that $E_J \lesssim E_C$ and $E_J, E_C \gg kT$. The drawing symbol for a mesoscopic junction is shown in Fig. 2(a). We will further assume that the bias source and the environment are small perturbations in the system [3]. For the unperturbed Hamiltonian (using appropriate terms in Eq. (1) and Eq. (3)) we get

$$H_0 = -\left(E_C \frac{\partial^2}{\partial \left(\Phi/2\right)^2} + E_J \cos\Phi\right). \tag{14}$$

Physically, the difference as compared to the previous section is, that the state of the junction can no longer be described with a single value of Φ. Overlap of wavefunctions corresponding to different minima in the washboard potential cause splitting of energy levels. In the infinite periodic potential this leads to formation of energy bands. This is in analogy to an electron in a solid-state crystal, where the periodic lattice forms the potential [8].

The time-independent Schrödinger equation $H_0\Psi = E\Psi$ is in this case mathematically a Mathieu differential equation. The energy eigenvalues are best represented in the basis of "quasicharge" $\widetilde{Q}$, a quantity analogous to crystal momentum in solid-state systems. In Fig. 2(b) we show the band structure in the limit $E_J \ll E_C$, the so-called weak-binding limit. In this Thesis we are using the extended band picture, where the lowest band is represented by $\left|\widetilde{Q}\right| < e$, the second band with $e < \left|\widetilde{Q}\right| < 2e$, etc. The voltage across the junction is given as

$$V = \frac{\partial E}{\partial \widetilde{Q}}, \tag{15}$$

and the expectation value of real charge is $Q = CV$. Thus the quasicharge $\widetilde{Q}$ agrees with Q at the

points, where the dashed parabola $E = \widetilde{Q}^2/2C$ coincides with the solid lines in Fig. 2(b). At $\widetilde{Q} = ne$ (with n an integer) the expectation value of Q is zero.

To understand the junction dynamics, let us first assume that the junction is initially at the lowest energy band at $\widetilde{Q} = 0$, and the junction is connected to an ideal constant current source with $I(t) = I_0$. If $I_0 \ll I_z \equiv \pi e E_J^2/8\hbar E_C$ (the criterion for adiabaticity), the quasicharge will increase up to $\widetilde{Q} = e$, return to $\widetilde{Q} = -e$ and finally back to $\widetilde{Q} = 0$. Repeating this cycle leads to coherent charge oscillation, i.e. the Bloch oscillation. The physical interpretation is that at $\widetilde{Q} = e$ a Cooper pair tunnels through the junction.

If I_0 is comparable to I_z, the criterion for adiabaticity is violated. Then interband tunneling at $\widetilde{Q} = ne$ (the Zener tunneling) becomes possible. The probability from band $n-1$ to band n is given as [9, 10]

$$P_{n-1 \rightleftharpoons n}^{Z} \approx \exp\left(-\frac{\pi}{8}\frac{1}{n^{2n-1}}\left(\frac{E_J}{E_C}\right)^{2n}\frac{eE_C}{\hbar I_0}\right). \tag{16}$$

In a realistic situation there are also mechanisms through which the system can return down to lower bands [11]. A way to provide controlled downwards relaxation is discussed in Section IV.

D. Electromagnetic environment

In this section we discuss the effect of ohmic dissipation for Cooper pair tunneling in mesoscopic Josephson junctions. We will be considering the circuit in Fig. 3(a), i.e. a junction voltage biased across a resistor R. We will now express the Hamiltonian of Eq. (1) as

$$H = H_J + H_{\text{env}}, \tag{17}$$

where H_J now represents the Josephson coupling and H_{env} now includes the contribution of both the capacitance of the junction as well as the circuit $\overline{Z}(\omega)$ parallel to the junction. In this case it is simply the resistor R. The environmental Hamiltonian can be represented as an infinite number of harmonic oscillators [12]. Josephson coupling H_J is now considered as a perturbation in the system. The tunneling through the junction is calculated by using the Fermi golden rule [13, 14, 15], where the rate between initial and final states ($|R>$ and $|R'>$, respectively) is given as $\Gamma_{R\rightarrow R'} = (2\pi/\hbar)\left|\langle R'|H_J|R\rangle\right|^2 \delta(E_R - E'_R)$, where $\langle R'|H_J|R\rangle$ is the matrix element describing the transition, and E_R and E'_R are the energies corresponding to initial and final states. We get the total rate by summing over all possible initial and final states, i.e.

$$\Gamma(V) = \frac{2\pi}{\hbar}\sum_{R,R'}\left|\langle R'|H_J|R\rangle\right|^2 P_\beta(R)\,\delta\left(E_R - E'_R\right), \tag{18}$$

where $P_\beta(R)$ is the probability of finding the system initially at state R. By assuming that the environment is at thermal equilibrium (i.e. that $P_\beta(R) = \langle R|\rho_B|R\rangle$, where ρ_B is the equilibrium density matrix), it can be shown that [15]

$$\Gamma(V) = \frac{\pi E_J^2}{2\hbar} P'(2eV), \tag{19}$$

where the direction of tunneling is taken towards positive voltage in Fig. 3(a). The rate to the opposite direction is obtained by reversing the bias voltage. The function $P'(E)$ is given as

$$P'(E) = \frac{1}{2\pi\hbar} \int_{-\infty}^{\infty} dt \exp\left[J(t) + \frac{i}{\hbar} Et\right]. \tag{20}$$

Here $J(t) = \langle [\Phi(t) - \Phi(0)] |\Phi(0)\rangle$ is the phase-correlation function. It can be shown to be [15]

$$J(t) = 2 \int_0^{\infty} \frac{d\omega}{\omega} \frac{R/R_Q}{1 + (\omega RC)^2} \left[\coth\left(\frac{1}{2}\frac{\hbar\omega}{k_B T}\right)(\cos(\omega t) - 1) - i\sin(\omega t)\right], \tag{21}$$

where $R_Q = h/4e^2$ is the quantum resistance for Cooper pairs.

If the charge relaxation time RC in the circuit of Fig. 3(a) is small compared to the average time between consecutive tunneling events, a current-voltage curve is simply $I(V) = 2e(\Gamma(V) - \Gamma(-V))$. However, in many cases this is not the situation. In this Thesis we have adopted an approach, where we integrate the charge across junction electrodes as function of time from

$$\frac{dQ}{dt} = \frac{1}{R}\left(V - \frac{Q}{C}\right) + \left(\frac{dQ}{dt}\right)_{CP}, \tag{22}$$

where the first term is the current through R. Here we have assumed that the voltage across the junction is Q/C. It is equivalent to assume that the quasicharge is the real charge at all times (see Eq. 15). This is approximately true in the limit of small E_J/E_C, where the junction energy roughly follows the parabolic dependence at almost all values of quasicharge (see Fig. 2(b)). The second term changes the charge by $2e$ every time a Cooper pair tunnels through the junction. The corresponding time dependent tunneling rate is obtained from Eq. (19) by setting $V = Q/C$.

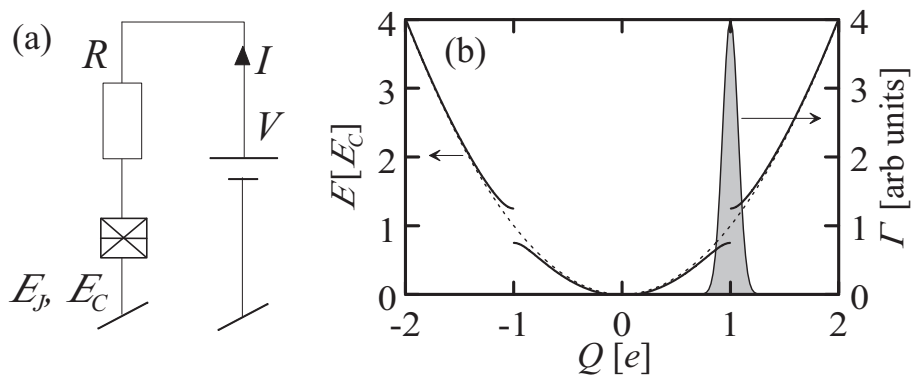

Figure 3. (a) A mesoscopic Josephson junction voltage biased across resistance R. (b) The peaked tunneling probability for large R shown on top of the band diagram.

It is useful to discuss the relation between the band model derived in the previous section and the model derived here. In the limit of large impedance ($R/R_Q \gg E_C/kT$), function $P'(E)$ can be calculated analytically, and stands

$$P'(E) = \frac{1}{\sqrt{16\pi kTE_C}} \exp\left(-\frac{E_C}{16kT}\left(\frac{E}{E_C} - 4\right)^2\right), \tag{23}$$

i.e. it is a Gaussian distribution centered at $E = 4E_C$. The width is determined by the thermal energy kT. The tunneling rate from Eqs. (19) and (23) is shown in Fig. 3(b). It is peaked at $Q = e$. If the bias voltage is set to $V \gtrsim e/C$, the charge relaxes towards $Q = CV$. As the state passes through $Q \approx e$ it is likely that a Cooper pair tunnels through the junction returning the state back to $Q \approx -e$. We have thus recovered the picture of Bloch oscillations by interpreting $|Q| \lesssim e$ as the lowest band. The difference is that now the Cooper pairs do not tunnel strictly at $Q = e$, which is due to fluctuations of R. The oscillations are no longer strictly coherent, but have a finite bandwidth.

If we further simplify Eq. (23) by assuming that $E_C/kT \gg 1$ and use Eq. (19) we get

$$\Gamma'(Q) = \frac{\pi e E_J^2}{8\hbar E_C}\delta(Q - e) \tag{24}$$

by expressing the rate in terms of charge (i.e. $\Gamma(V) = \Gamma'(Q)$). During a period of Bloch oscillations the tunneling rate is thus $\Gamma = \left(\pi e E_J^2/8\hbar E_C\right)/\Delta Q$ for a very short time Δt, i.e. while $e - \Delta Q/2 < Q < e + \Delta Q/2$. If the current at $Q = e$ is I_0, we can write $\Delta Q = I_0 \Delta t$, so $\Gamma = \left(\pi e E_J^2/8\hbar E_C I_0\right)/\Delta t$. The probability distribution of tunneling is exponential $\Gamma \exp(-\Gamma t)$. The total probability of Cooper pair tunneling during the period is thus

$$P_{CP} = \int_0^{\Delta t} \Gamma \exp(-\Gamma t)\, dt = 1 - \exp\left(-\frac{\pi}{8}\left(\frac{E_J}{E_C}\right)^2 \frac{eE_C}{\hbar I_0}\right). \tag{25}$$

Zener tunneling is complementary to Cooper pair tunneling, i.e. $P^Z_{0\rightleftharpoons 1} = 1 - P_{CP}$. Thus, for the two lowest bands ($n = 1$) the result of Eq. (16) is recovered. Cooper pair tunneling at upper bands is not included. This is justified for small E_J/E_C, since $P^Z_{n-1\rightleftharpoons n}$ is very close to unity for $n > 1$.

In conclusion, for large resistances R, low temperatures, and small Josephson coupling the dynamic model derived in this section is equivalent to the band model of the previous section. As an extension it takes into account environmental fluctuations due to R.

3. Josephson voltage standards

A. Background

In the original article by Josephson [1] it was predicted that a junction, when irradiated by microwaves having frequency f (the pump frequency), would exhibit a constant average voltage

$$V_{ave} = n \times f/K_J \tag{26}$$

over a range of DC bias currents determined by the amplitude of the irradiation. Here n is an integer and $K_J = 2e/h \approx 4.83 \times 10^5$ GHz/V is the Josephson constant.

The phenomenon is understood in terms of phase locking the Josephson oscillation with the external microwave signal. In reference to the dynamical model in Section IIB and Fig. 1(b) the phase-locking corresponds to a situation, where the washboard potential is periodically tilted with frequency f. If the bias parameters and the parameters of the junction are properly selected, the phase advances exactly $2\pi n$ during one microwave period $1/f$. From Eq. (6) this leads to average voltage

$$V_{ave} = \frac{1}{1/f}\int_0^{1/f} \frac{\Phi_0}{2\pi}\frac{d\Phi}{dt}dt = f\int_0^{2\pi n}\frac{\Phi_0}{2\pi}d\Phi, \tag{27}$$

which reproduces Eq. (26). Solutions of dynamic equations (Eqs. (6) and (7)) of this type are called harmonic. Other possible solutions are subharmonic, where during m microwave periods the phase advances $2\pi n$, i.e. $V_{ave} = (n/m)\, f/K_J$, or chaotic, where the dynamics is completely aperiodic. The conditions for harmonic phase locking are widely studied theoretically in case of the simple resistively shunted junction [6],[16]-[19]. In section IIIB we will study the conditions for the circuit of another realization.

Constant voltage steps were first experimentally measured by Shapiro in 1963 [20]. In 1967 Parker et. al. measured the value of K_J with uncertainty of about 6 parts per million (ppm) using many different types of weak links [21]. The largest source of error was the inaccuracy of the realization of the absolute volt at the time. Within the measurement uncertainty of the experiment (2 ppm) the values of K_J were reproduced for both superconductor-oxide-superconductor and point contact weak links fabricated from various materials. This suggests that the frequency-to-voltage conversion is highly independent on the experimental details. Therefore the phenomenon has been adopted to use in metrology, and today the Josephson voltage is the most commonly used practical realization of the volt.

The problem with a single junction is the low voltage it produces at realistic frequencies. This causes several problems. It is difficult to calibrate out possible error voltages, e.g. thermal voltages in the measurement leads. Practical calibrations are also often done at 1 - 10 V level, and the required voltage dividers cause additional uncertainty. For a single junction voltage standard together with a divider calibrated by means of a cryogenic current comparator the relative uncertainty at 1 V level has been brought down to 10^{-8} [22].

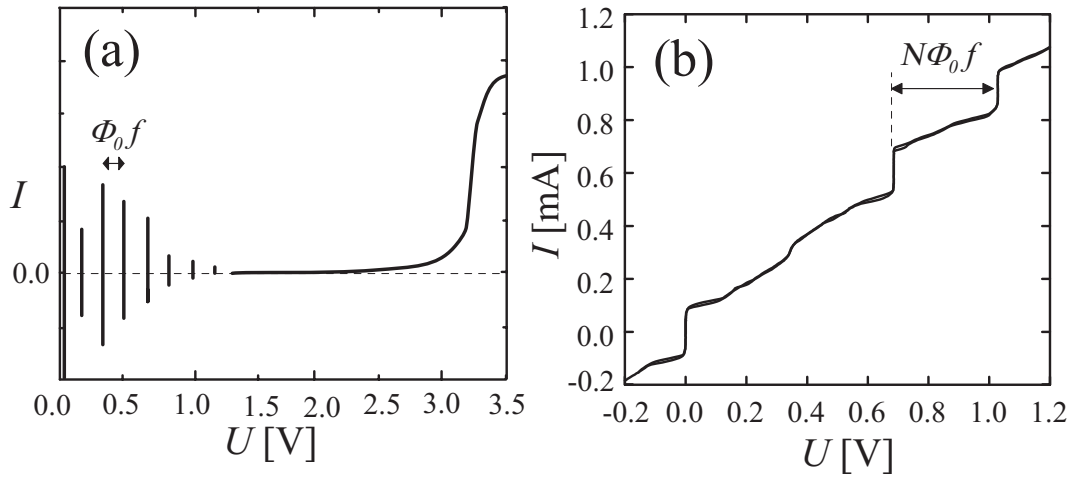

Figure 4. (a) A schematic IV curve of a conventional Josephson voltage standard irradiated with frequency f. The spacing of different voltage levels is exaggerated for clarity. (b) A measured IV curve from a VTT programmable Josephson standard.

The development of junction fabrication techniques has made it possible to increase the voltage by connecting several junctions in series. Today practical 1 - 10 V DC references are based on arrays of typically 2000 - 20000 series connected junctions irradiated with $f \approx 70$ GHz [23]-[25]. Thus they directly produce the required output voltage. The junctions are undamped superconductor - insulator - superconductor (SIS) junctions. An IV curve of an undamped Josephson array under microwave irradiation is schematically shown in Fig. 4(a). It is highly hysteretic, since for high quality junctinons the subgap leakage resistance is very high. This increases the hysteresis parameter β_c (see Eq. 8). The quantized voltage across the junction can exist without DC bias current. The steps are thus called zero-crossing steps.

The zero-crossing steps have some advantages. The absence of bias current makes the output voltage insensitive to possible additional series resistance. In case of arrays it also alleviates the fabrication criteria, since the variation of damping resistance does not cause problems. They have some disadvantages as well. They are very sensitive to environmental interference. The output voltage is not a single-valued function of bias parameters, but rather depends on the initial conditions of the dynamic equations (Eq. (8)). Therefore the interference can cause transitions between different voltage steps making the requirement of electromagnetic shielding strict. Low damping also makes the selection of the desired output voltage slow and tricky, which makes it more difficult to automate measurements. It also prevents the direct use of the Josephson voltage in AC calibrations.

The drawbacks of zero-crossing voltage standards has lead to development of programmable Josephson arrays based on damped junctions [26]. They are both faster and more stable than the conventional arrays. Working programmable voltage standards at 1 volt level have been fabricated using intrinsically damped junctions. In them the damping is provided by a dissipative material in the junction barrier. Suitable junctions are superconductor - normal- superconductor (SNS) [27] or superconductor - insulator - normal - insulator - superconductor (SINIS) junctions [28] .

In this thesis we discuss another approach, where SIS junctions are damped with external shunt resistors. A one volt programmable Josephson voltage standard has been developed as part of the thesis. An example IV curve from such an array is shown in Fig. 4(b).

B. VTT programmable voltage standard

In this Section we present design and experiments of the VTT arrays. In addition, we present a general optimization procedure for programmable arrays based on externally damped SIS junctions. The aim is to answer the question of how to design an array for a given voltage level, which is stable against external fluctuations, has low power consumption, and is fast.

A photograph of a one volt VTT Josephson voltage array chip is shown in Fig. 5(a). The main parts are generally similar to those used in conventional zero-crossing voltage arrays (see e.g. [29]). The fin-line taper provides a transition from a waveguide into on-chip superconducting microstriplines, which are used to guide the 70 GHz microwave signal into the Josephson junctions. The off-chip waveguide is in this case a rectangular E-band waveguide (WR-12). After the fin-line taper the microstriplines form a power distribution network, which guides the signal into parallel paths connected to junction chains. The power distribution network is formed by a cascade of matched T-junctions, where each junction divides the incoming signal into two outgoing signals of equal power. The junctions are also in a microstripline configuration, where the hotline is formed by the junction chain and the groundplane is a superconducting plate (Fig. 5(b)). The JJ chains are organized in branches, which are parallel with respect to the incoming microwave power. After the chains the microwave is guided into terminations. They are also microstriplines, but with normal conducting hotlines. They are long enough to dissipate most of the incoming power. This is to prevent standing waves due to reflections, which guarantees homogeneous microwave power for all junctions. At low frequencies the junction chains are connected in series to sum the voltages from different branches. The frequency separation is provided by filtering, i.e. DC block capacitors to isolate the power distribution network from low-frequency signals and low-pass filters to prevent microwave signals to couple from one branch to another.

The fabrication process is the VTT niobium trilayer process, which with some modifications has been successfully used to fabricate SQUIDs [30] for over a decade [31]-[35]. The devices are fabricated on 100 mm silicon wafers. Patterning is done by photolitography and either by reactive ion etching (Nb layers) or wet-etching (SiO_2 and Mo layers). The layer structure is visualized in Fig. 5(b), where the junction structures as well as other superconducting and insulating layers are shown. The lowest layer, sputtered Nb, forms the superconducting groundplane. The next layer is an insulator, which forms the dielectric for the microstriplines. It is SiO_2 grown with plasma enhanced chemical vapor deposition (PECVD). On top of this there is the trilayer, a Nb-Al-AlO_x-Nb -layer containing the Josephson junctions. It is formed by sputtering the base Nb, on top of which a thin ($\sim$5 nm) Al-layer is deposited. The tunnel barrier AlO_x ($\sim$2nm) is then formed by exposing the aluminium to oxygen for a given time at a constant pressure. On top of the oxide, a Nb counter electrode is grown . The junctions are then defined by anodizing the area around the junctions forming a zone of Nb_2O_5 around them. The counter electrode is

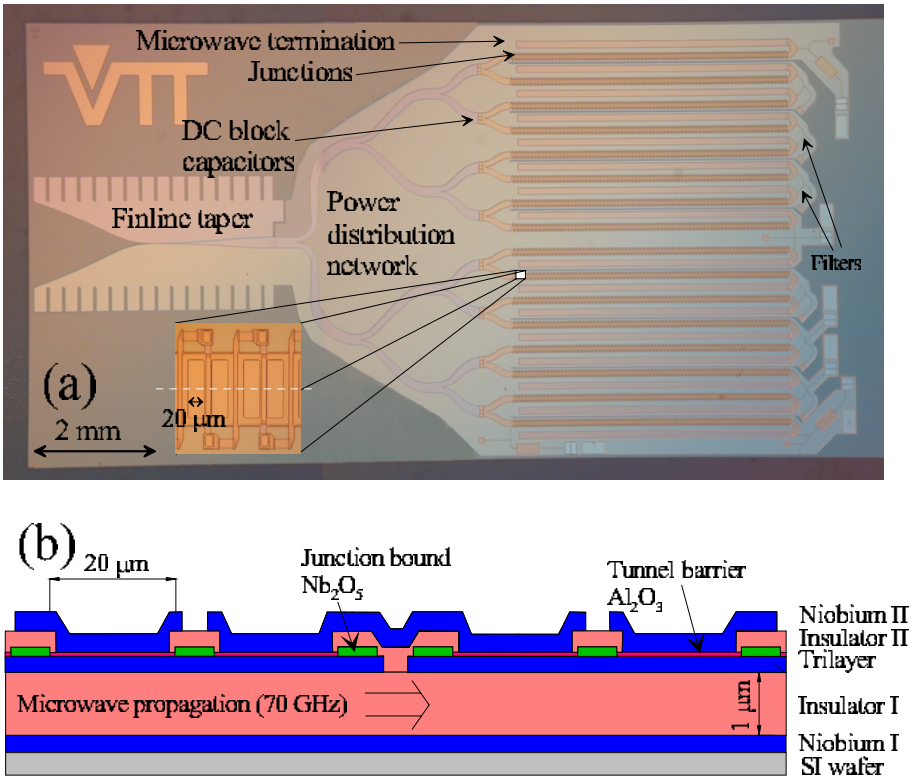

Figure 5. (a) An optical microscope photograph of a VTT programmable voltage standard (design 1(a)). Main parts of the circuit are indicated. The magnification shows a part of a junction chain. (b) A cross section from the junction chain. The aspect ratio is altered for clarity.

then removed excluding the junction areas. For the wiring, additional layers of SiO_2 and Nb are deposited. The last layers (not shown in the figure) are the resistor layer (sputtered molybdenum forming the shunt resistors and microwave terminations) and the passivation layer SiO_2 to protect the on-chip components.

In order to produce a stable quantized voltage, the microwave distribution along the branches must be sufficiently homogeneous. To achieve this, our approach is to minimize the attenuation of the shunt resistors by blocking the microwave signal from the resistor by an inductor L. The circuit is shown schematically in Fig. 6(a) and the realization in 6(b). We first study the intrinsic stability criteria. By intrinsic stability we mean here that a quantized voltage (Eq. (26)) appears as a single-valued function of bias current for as large a range of bias currents as possible. For a junction, which satisfies the simple RCSJ-model (Eq. (8)), the step amplitude (i.e. the range ΔI_n of bias current I_0, at which the quantized voltage state can appear) is [17]

$$\Delta I_n = 2I_c \left| J_n \left(\frac{I_1}{2\pi\Phi_0 f^2 C} \right) \right|, \tag{28}$$

where I_1 is the amplitude of the pump current. Here it has been assumed $(\omega C)^{-1} \ll R$, where $\omega = 2\pi f$ is the angular pump frequency. This is typically always satisfied for SIS junctions. The index n corresponds to the step index n in Eq. (26).

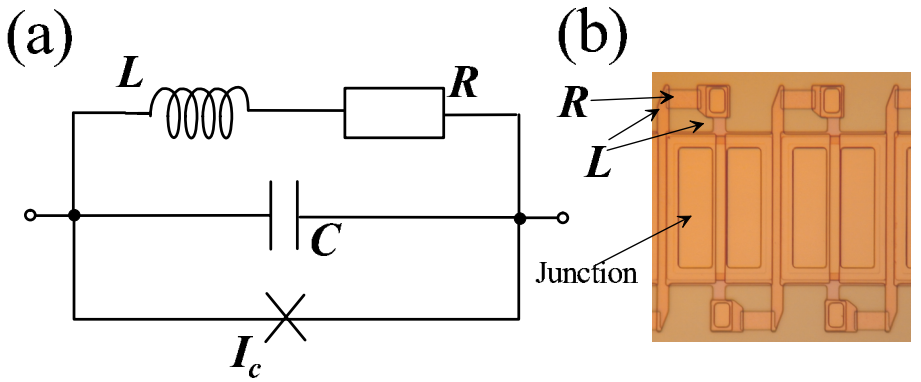

Figure 6. (a) The circuit with frequency dependent damping (schematically) and (b) the realization.

We quantify the criterion for intrinsic stability so that the effective step amplitude of our circuit in Fig. 6 is not substantially suppressed from the value of Eq. (28). The method to analyze the problem is solving Eqs. (6) and (7) numerically as in Ref. P2. The parameter space to be mapped is defined by the hysteresis parameter β_c (see Section IIB), the dimensionless inductance $\beta_L = 2\pi L I_c/\Phi_0$, and the dimensionless angular frequency $\Omega = (\Phi_0/2\pi I_c R)\,\omega$.

The data from such simulations is collected in Fig. 7. In Fig. 7(a) each triangle represents a result from a simulated IV curve. The triangles pointing upwards indicate points, where the simulated step amplitude satisfies Eq. (28). The triangles pointing downwards indicate points, where the simulated step amplitude is suppressed from this value. The main objective was to find a criterion for β_L. Therefore especially the boundary, where the increasing inductance begins to cause decreased stability, was mapped. Each pair of triangles thus illustrates the boundary of stable (below) and unstable (above) region. The resulting certainly stable region is shown grey in Fig. 7(a), where also the conventional criterion, that the pump frequency exceeds the plasma frequency [17]

$$\Omega\sqrt{\beta_c} \gtrsim 3 \tag{29}$$

was adopted. Although it was originally derived for undamped junctions, it was found to apply here as well.

Even though the stable region of Fig. 7(a) guarantees the existense of the quantized voltage state with a wide range of bias currents, it does not yet guarantee, that the voltage is a single valued function of current. To avoid constant voltage steps with different indices n to become overlapping (in the same sense as in zero-crossing steps, see Fig. 4(a)), the criterion is (see e.g. Ref. [27])

$$\Omega \gtrsim 1. \tag{30}$$

On the other hand, a resistive solution can coexist with the quantized voltage state (see e.g. the insets of Fig. 7). To avoid this, a set of simulations was executed to find out how this affects the effective step amlitude. The data is summarized in Fig. 7(b). It can be seen, that sufficient

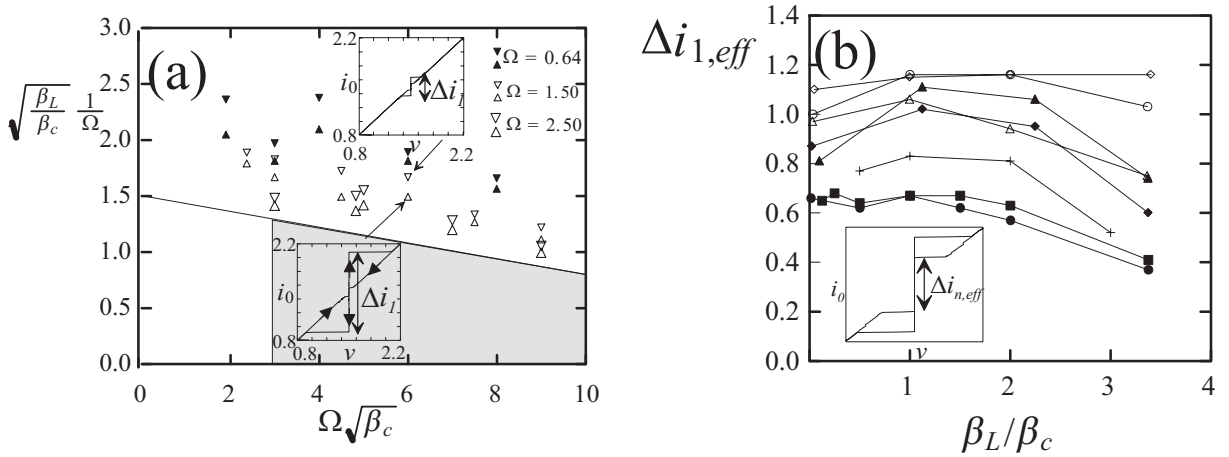

Figure 7. Stability data from numerical simulations. (a) Triangles pointing upwards mark IV curves with large step amplitudes ΔI_1 (the lower inset). Those pointing downwards mark IV curves with suppressed amplitudes due to chaotic behavior (the upper inset). The insets are examples of simulated IV curves. The arrows of the lower inset also shows the trajectory as the current is swept up and down. The area shown in gray is the certainly stable region of parameters. (b) The effective step amplitude (see the inset for the definition) for different parameters and step $n = 1$. Parameters for open diamond: $\Omega = 1.5$, $\beta_c = 2.0$, open circle: $\Omega = 1.5$, $\beta_c = 3.0$, solid triangle: $\Omega = 1.5$, $\beta_c = 4.0$, cross: $\Omega = 1.5$, $\beta_c = 6.0$, solid square: $\Omega = 1.5$, $\beta_c = 8.0$, open triangle: $\Omega = 2.5$, $\beta_c = 3.0$, solid diamond: $\Omega = 2.5$, $\beta_c = 4.0$ and solid circle $\Omega = 2.5$, $\beta_c = 8.0$.

criteria in practice are

$$\beta_c \lesssim 4 \tag{31}$$

$$\beta_L \lesssim 2\beta_c, . \tag{32}$$

The criterion of Eq. (31) together with Eqs. (29) and (30) also in practice guarantees that the stable region of Fig. 7(a) is reached.

To study the homogeneity of the pump current, analysis of the circuit in Fig. 8(a) (see Ref. P2) gives for the pump signal attenuation

$$\alpha = \alpha_c \left(\frac{sl_0}{L}\right)^2 + \alpha_d, \tag{33}$$

where $\alpha_c = (1/2)\, R/Z_0$ is the attenuation in the absence of frequency separation, s is the length of the microstripline occupied by one junction, l_0 is the microstripline inductance per unit length and α_d is the dielectric attenuation of the microstripline.

The optimization is performed assuming the simplified geometry shown in Fig. 8(b). The figures of merit are the output voltage U_{out}, the required microwave power P_{in}, the speed described by the time constant of the array τ_{RC}, and the step width ΔI_n. The speed is essential in precise AC voltage generation and the step width is a measure of stability against external fluctuations due to the environment and the measurement circuitry. Demanding that the intrinsic stability criteria (Eqs. (29)-(32)) apply, and that the attenuation (Eq. (33)) does not significantly suppress the step width, we can write the figures of merit in terms of design parameters. These are junction

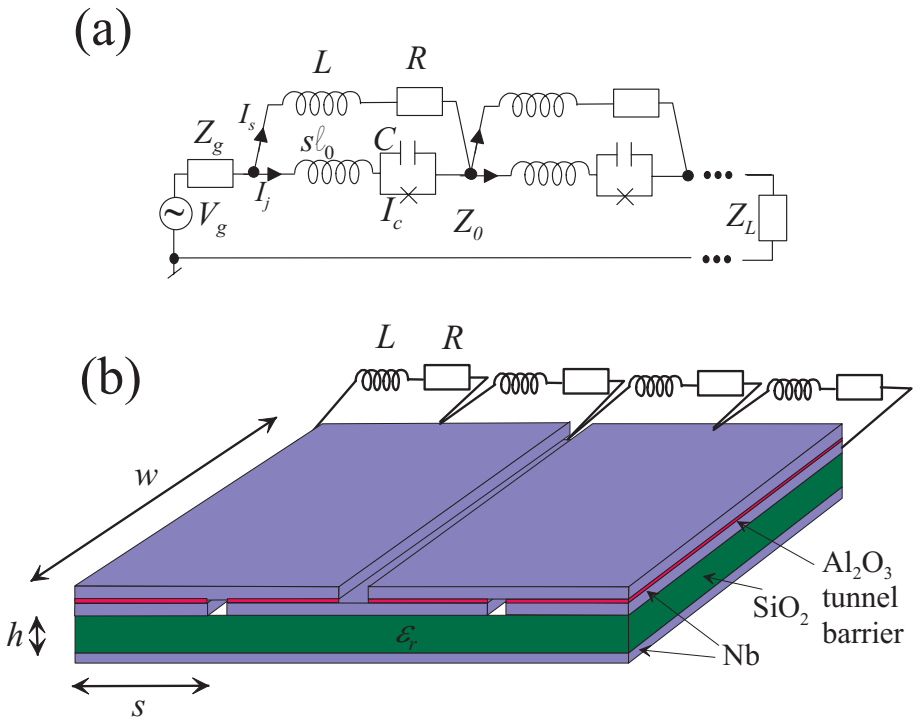

Figure 8. (a) The circuit diagram of the junctions embedded in the transmission line. (b) The simplified geometry assumed in the optimization procedure.

and microstripline dimensions w, s, h (see Fig. 8(b)), number of branches M, number of junctions N, and the step number n. It follows

$$U_{out} = Nn\Phi_0 f \tag{34}$$

$$\Delta I_n = \frac{4}{\pi}\frac{j_c w s}{\sqrt[3]{n}} \tag{35}$$

$$P_{in} = M\rho\left(1+n\right)^2 hws^2 \tag{36}$$

$$\tau_{RC} = N^2\gamma\frac{1}{h} \tag{37}$$

$$\frac{N}{M}\left(\kappa h s^3 + \alpha_d s\right) \lesssim \ln\left(1+\frac{1}{n}\right), \tag{38}$$

where the last line is the remaining criterion for the attenuation, which needs to be satisfied. Here j_c is the critical current density, which should be maximized while keeping Eq. (29) valid. In physical units this leads to $j_c = 2\pi\Phi_0 c_s \left(f/3\right)^2$, which is nearly constant for a given pump frequency and a fabrication process. The junction capacitance per unit area c_s is nearly constant for a given tunnel barrier material. Other constants are $\gamma = \left(2/3\pi^2\right)\Phi_0 f\varepsilon_0\varepsilon_r/j_c$, $\rho = 2\sqrt{\mu_0/\varepsilon_0\varepsilon_r}\pi^2\Phi_0^2 f^4 c_s^2$ and $\kappa = \left(3j_c/4\Phi_0 f\right)^3\sqrt{\mu_0^3\varepsilon_0\varepsilon_r}/c_s^2$.

Approximating $\ln\left(1+1/n\right) \approx 1/n$, and assuming that $\alpha_d \approx 0$, we can find the general trade-off for the optimized design as

$$\tau_{RC} \propto \frac{n+1}{n^{7/6}} \frac{1}{f^5} \frac{(U_{out}\Delta I_n)^{5/2}}{\sqrt{P_{in}}}, \tag{39}$$

which indicates that an array cannot be speeded up beyond a limit without either using more input power, or dropping the output voltage. The situation can be slightly improved with increasing the step number n, but the dependence is very weak. However, operating the device at higher steps has the practical advantage of decreasing the number of junctions needed.

In addition to the design, the devices set strict criteria to the fabrication process. For example, a one volt array pumped with $f = 70$ GHz needs about 2300 series connected Josephson junctions. Each of these needs to be fabricated flawlessly. In other words the yield of Josephson junctions needs to be at least 99.96% for an array to work. The critical current spread needs to be at a tolerable value, since at metrological measurements the smallest critical current determines the step amplitude and thus the stability against external fluctuations. Also the scatter in the shunt resistance needs to be very small. In the presence of resistance scatter the quantized voltage state is obtained at different bias currents for different junctions, which decreases the effective step amplitude (see Ref. P1).

As part of this Thesis, two main versions of arrays aimed to work at about 1 V level were designed and tested at DC. The first design (Ref. P1) is aimed to produce the voltage of 1 V (design 1a) or 1.5 V (design 1b) at step $n = 3$. A photograph of an array with design 1a is shown in Fig. 5(a). The second design (design 2) (Ref. P3) has two identical arrays integrated on the same chip with a single microwave input. Both subarrays produce an output of about 1.5 V at step $n = 3$. A photograph and a schematic circuit arrangement are shown in Fig. 9. Design 1 was made before the optimization procedure above was developed, while in design 2 the optimization was utilized.

The room temperature electronics of the experimental setup consisted of 70 GHz electronics, a DC bias source (typically Fluke 5700 calibrator in series with resistance of 5 - 50 kΩ) and a voltmeter. In high precision measurements, HP 3458A digital voltmeter was used to verify the step flatness with a resolution of ∼100 nV. A cryoprobe was designed for cooling the chip down to 4.2 K. For the pump signal, the probe has a waveguide transition from WR-12 waveguide into an oversized circular waveguide at the room temperature end. At the cold end there is

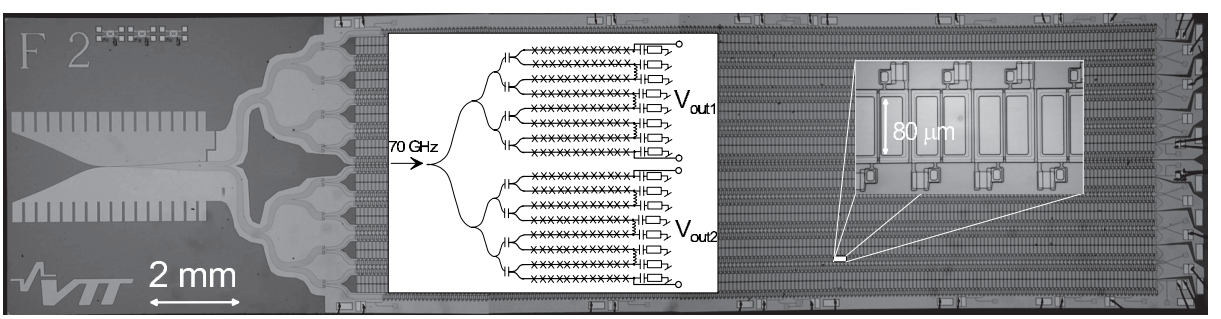

Figure 9. A microscope photograph of an array with design 2. Insets show the wiring arrangement with two independent output voltages and a magnification from a junction chain.

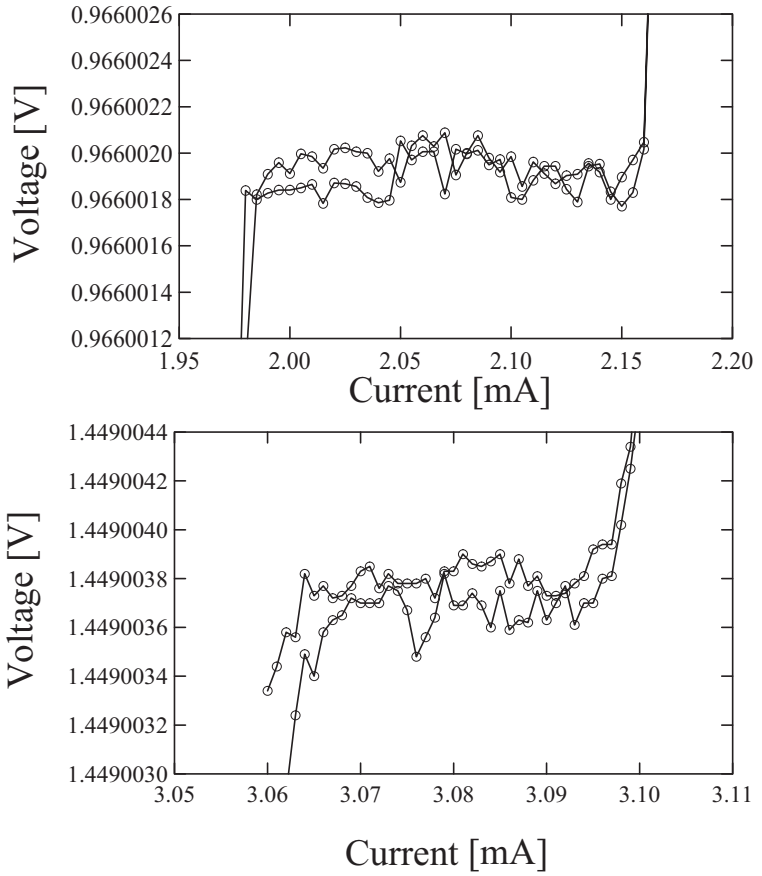

Figure 10. Quantized voltage states measured with an array of design 2. (a) Step $n = 2$ and (b) Step $n = 3$.

another transition from the oversized waveguide back to WR-12 guide, which has a slot for the finline taper of the chip. The DC lines (twisted copper pairs) were filtered with *RLC*-filters at room temperature. The 70 GHz electronics was a part of the standard JVS calibration setup of the Centre for Metrology and Accreditation and (MIKES). It consists of a Gunn diode as the microwave source. It is operated in a phase-locked loop consisting of an EIP-578B frequency counter with a 110 GHz extension. The frequency reference is traceable back to the Cs atomic clock of MIKES.

An IV curve from a chip with design 1a is shown in Fig. 4(b) at a rough voltage scale. At more accurate measurements the constant voltage steps with $n = 1$ and $n = 2$ showed flat steps. The one volt steps with arrays of design 1b and $n = 2$ showed effective step amplitudes typically between 60 – 100 μA. The third constant voltage step, however, has not been found flat in measurements having a resolution below 1 μV. An array with design 1b also took part in an international intercomparison measurement (Euromet project 626 [36]), where the array output at about 0.5 V and 1 V levels were compared against conventional SIS-arrays. In direct comparisons an agreement better than 0.4 nV was achieved.

The optimization algorithm presented above was utilized in design 2. The problem of degrading step amplitude with increasing step index n is possibly due to the variation in the shunt resistance.

An attempt to decrease the scatter was made by sputtering the resistor films in a mode, where the sample stage was oscillating. The aim of this was to decrease thickness variations of the resistor film. The resistors were characterized by measuring a large quantity of room temperature test structures aiming to clarify both the contribution of the film thickness and the line width. From the set of experiments an estimate was made, that ΔR should be below 4%.

Resulting IV curves are shown in Fig. 10. Shown are the steps $n = 2$ and $n = 3$ taken from measurements having resolution of about 200 nV. Flat constant voltage steps are obtained in both cases. With $n = 2$, the effective step amplitude at 1 V level is about twice the value obtained from design 1, even though the power consumption per subarray is about one half, and the rise time is of the same order as in design 1. The step $n = 3$ shows flat steps for this design as well. However, a practical problem has been the low yield of arrays, and by the date only one working array has been found to produce flat voltage steps at a metrological accuracy. A probable reason is the variation of critical current density between different arrays. It was also later found, that an additional design criterion is imposed to prevent the self-generated power of the junctions from causing pump signal inhomogenity [37]. This makes the criterion for the scatter more restrictive.

The main application of the arrays is a calibration setup for tracing an AC voltage back to the Josephson voltage. This can be done in a more direct way than with conventional methods. A possible method for doing this is introduced in Ref. [38] and the practical setup is being developed as collaboration of MIKES and VTT. Two arrays in a bridge configuration can also be utilized in arbitrary impedance intercomparisons (Ref. P3). In this case the array with two independent outputs (design 2) is useful. The main requirement for AC applications is the speed. For an AC waveform of frequency f_s, the error due to transients as limited by the array is (Ref. P2)

$$\frac{\Delta U}{U} = 2\pi^2 \left(\tau_{RC} f_s\right)^2 . \tag{40}$$

For $f_s = 1$ kHz both designs should enable an uncertainty as low as about 0.1 ppm. An additional challenge is whether the array tolerates the level of noise introduced by the fast bias electronics. Experiments made with arrays of design 1 have confirmed that $\tau_{RC} \lesssim 250$ ns, which is still likely to be limited by the setup [39, 40]. Preliminary experiments with AC generation suggest that also the steps remain flat at least within 1 ppm with the fast bias electronics.

4. The Bloch oscillating transistor

A. Amplifiers based on mesoscopic tunnel junctions

Development of nanofabrication techniques has led to a new family of devices, in which the charging energy $\sim e^2/2C$ of a single charge carrier (either an electron in a normal conductor or a Cooper pair in a superconductor) is an important energy scale. The one most extensively studied is the single electron transistor (SET), which consists of two normal tunnel junctions connected to a normal conducting island having small capacitance C such that $e^2/2C \gg kT$ [41] -[43]. The Coulomb blockade of the island is tuned by an additional gate electrode, which in turn changes the current through the junctions. The SET has been found to be a highly sensitive electrometer [42, 44]. Also its superconducting counterpart, the single Cooper pair transistor (SCPT) provides comparable sensitivity [45]. Both devices have a gate-controlled island, which causes sensitivity to background charge fluctuations. This is seen as a high level of $1/f$ noise. To enhance the band (usually limited by the wiring of the cryostat in low-frequency applications) beyond the $1/f$-corner, varous RF readout techniques have been developed for the two-junction devices [46, 47], or a single junction embedded in a tank circuit [48].

In the gate-controlled devices the input signal is coupled capacitively to the device. In this sense they resemble the field effect transistor (FET) among semiconducting devices. The properties of FETs are crucially different from the bipolar junction transistors (BJTs), which have a resistive input and which essentially detect current. Among devices based on mesoscopic tunnel junctions, the resistively coupled SET (R-SET) has a resistive input impedance, though its performance has been found to suffer strongly from thermal fluctuations [49]. In this Thesis we analyze a new device, the Bloch Oscillating Transistor (BOT). It is based on controlling Cooper pair current in a single mesoscopic Josephson junction by means of quasiparticle current through a normal tunnel junction. Instead of controlling the static charge on the island, the tunneling quasiparticles induce interlevel transitions, which in turn affect the strength of the Coulomb blockade.

B. Principle of operation

The circuit of the Bloch oscillating transistor is schematically shown in Fig. 11(a). In addition to the basic mesoscopic Josephson junction voltage biased across a large resistor (see Section IID) there is an additional tunnel junction connecting a superconducting "island" to the base electrode (B). The base electrode is normal conducting, i.e. the base junction is a NIS or a NIN junction depending on the realization. The other two electrodes are named the collector (C) and the emitter (E). In the basic mode of operation the BOT is biased to a voltage $V_C \gtrsim e/C$, which makes the Bloch oscillations possible. They lead to a net charge flow through the collector-emitter circuit. The Bloch-oscillations are occasionally interrupted by Zener tunneling causing the transition into the second band, where the Cooper pair flow is blocked. We assume further that Cooper pairs tunnel only at the lowest band. This is justified in case of small Josephson coupling since the Zener tunneling probability between the upper bands is close to unity (see Eq. 16). We will thus refer to the system as a two-level system, and refer to the Bloch-oscillating

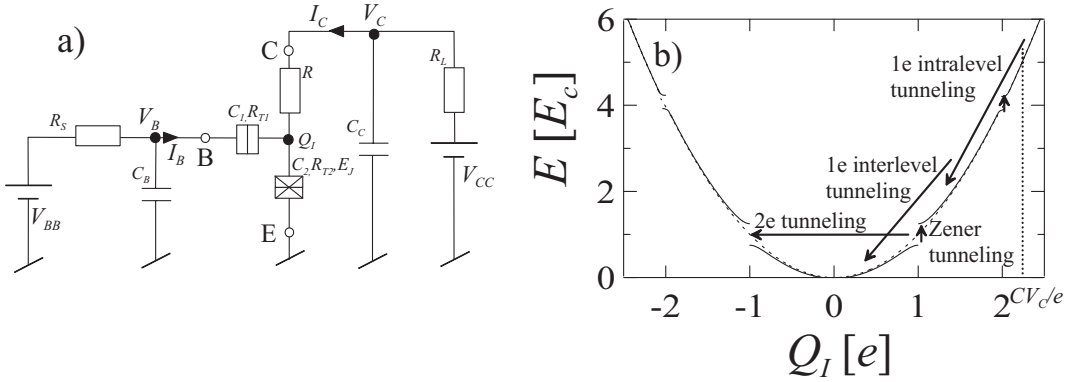

Figure 11. (a) The circuit of the Bloch oscillating transistor connected to source and load resistances R_S and R_L. Shown are also the lead capacitances C_B and C_C. (b) The band structure with possible transitions. The quasiparticle tunneling events through the base junction are shown in addition to transition mechanisms present in a bare mesoscopic JJ as well.

state (the lowest band) as the first level and the upper bands as the second level.

The transition from the second level down to the first one occurs via quasiparticle tunneling through the base junction. If the charge is initially $Q < 2e$, one quasiparticle always suffices to cause an interlevel transition. For $Q > 2e$ at least two electrons are needed, which leads to intralevel transitions within the second level (see Fig. 11(b)). The quasiparticle tunneling probability can be adjusted by changing the bias voltage (or current) of the base electrode. Thus the share of time the system spends at the first level is also adjusted. Therefore the current at the collector-emitter circuit (or collector current I_C) is controlled from the base electrode leading to transistor-like characteristics and signal amplification.

C. Computational modelling

The principle of operation was first shown computationally using a model similar to that described in Section IIC (Ref. P4). Originally the impedance at the collector electrode was assumed to be an LR-circuit instead of the simple resistor as in Fig. 11(a). The charge dynamics of the Josephson junction were described by adiabatic charge flow within the lowest band occasionally interrupted by Zener tunneling, the probability of which was evaluated from Eq. (16). The quasiparticle tunneling rate through the base junction was obtained from the orthodox theory of single electron tunneling [47]. The model did not, however, include inelastic Cooper pair tunneling which is possible in case of finite temperature and/or finite impedance at the collector electrode. It was still possible to predict charge dynamics essentially similar to those described above. Qualitatively correct characteristic curves were predicted and the device was shown to have gain.

Due to realization issues the practical devices were fabricated without the extra inductance at the collector. To predict the device characteristics quantitatively, the effect of fluctuations due to the collector resistor needs to be accounted for. The solution was to use the model introduced in Section IID, i.e. the time dependent phase-correlation theory, which gives correct charge dynamics

also in case of finite collector resistance R_C and finite temperature. The model is extended to account for the quasiparticle tunneling as well (Ref. P6). It is summarized as follows. The "island" charge $Q_I = Q_2 - Q_1$ is integrated in the time domain as

$$\frac{dQ_I}{dt} = \frac{V_C - V_2}{R_c} - \left(\frac{dQ_I}{dt}\right)_{QP1} - \left(\frac{dQ_I}{dt}\right)_{QP2} - \left(\frac{dQ_I}{dt}\right)_{CP}, \tag{41}$$

where the first term describes the charge flow through the collector resistor, the second and third terms describe the effect of quasiparticle tunneling through the base junction and the JJ, respectively, and the last term is the Cooper pair tunneling through the Josephson junction. Tunneling rates for both quasiparticles and Cooper pairs are obtained from the $P(E)$-theory [15].

D. Comparison of experiments and simulations

The experimental BOT samples were fabricated and measured in the Low Temperature Laboratory of Helsinki University of Technology. They were fabricated using electron beam lithography and four-angle shadow evaporation technique. The JJ was an Al/AlO_x/Al -junction ($\sim$ 100nm $\times$ 100 nm), and the base junction had Al/AlO_x/Cu structure. The collector resistor was a narrow strip ($\sim$100 nm $\times$ 20 μm) made of a thin ($\sim$10 nm) layer of chromium. In some samples the JJ was fabricated in the SQUID geometry, which enables tuning of the Josephson coupling by an external magnetic field. The measurements were done in a dilution refrigerator at temperatures of about 100 mK.

Sets of computed collector current - collector voltage ($I_C - V_C$) curves together with corresponding experimental results are shown in Fig. 12. The sample parameters are presented in Ref. P6. Quantitative agreement is reasonably good. Differences appear particularly, when the Josephson coupling is large. This is the case especially with the sample in Fig. 12(b), where $E_J/E_C \approx 1.7$ as estimated from the experimental data. The computed peaks are at lower voltages and currents than the experimental ones. In this case Zener tunneling probability between the higher bands is below unity (Eq. (16) with $n > 1$). This indicates that Cooper pair tunneling at higher bands may have an impact to the experimental result. Also the assumption that quasicharge equals real charge is somewhat violated with $E_J/E_C \gtrsim 1$.

The computed dynamics of different samples at different points of operation are illustrated in Fig. 13. The corresponding points of operation are indicated in Fig 12. Regular BOT operation, i.e. the operation essentially similar to the original idea of BOT, is shown in Fig. 13(A1), where the quasiparticle current clearly enhances Cooper pair current. The inverted BOT-operation is shown in Fig. 13(A2), where quasiparticle tunneling tends to drive the Josephson junction out of the lowest band. The single-electron current thus suppresses Cooper pair current in this case. The nonsymmetric nature of the dynamics explains why $I_C - V_C$ curves are not symmetrical as the sign of V_C is reversed. It has been shown that substantial current gain is obtained for both regular and inverted operation.

The IV-curves of Fig. 12(b) are slightly hysteretic both in the experimental and the computational datasets. The time-domain plots of Fig. 13(B1) and (B2) illustrate the dynamics in

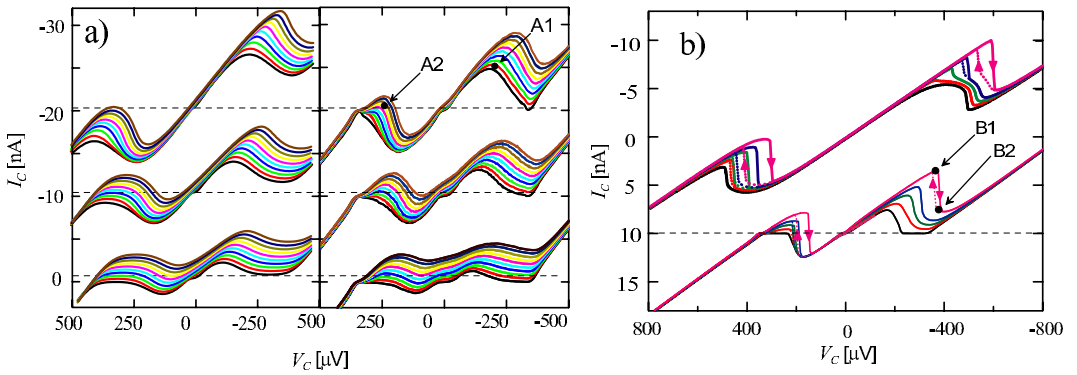

Figure 12. Simulated and experimental $I_C - V_C$ curves for two samples. The arrows denote points of operation, the dynamics of which are plotted in Fig. 13. (a) The sample has a SQUID geometry, and is measured with three different Josephson couplings (sets from down to top E_J/E_C=0.35, 0.7, 1.2). The upper sets are offset by -10 nA and -20 nA, respectively, for clarity. The data in the left frame is experimental and the right frame computational. (b) The sample has a constant Josephson coupling E_J/E_C=1.7. The upper set is experimental and the lower set (offset by 10 nA) is computational. Both in (a) and in (b), different curves in each dataset are measured with different base currents.

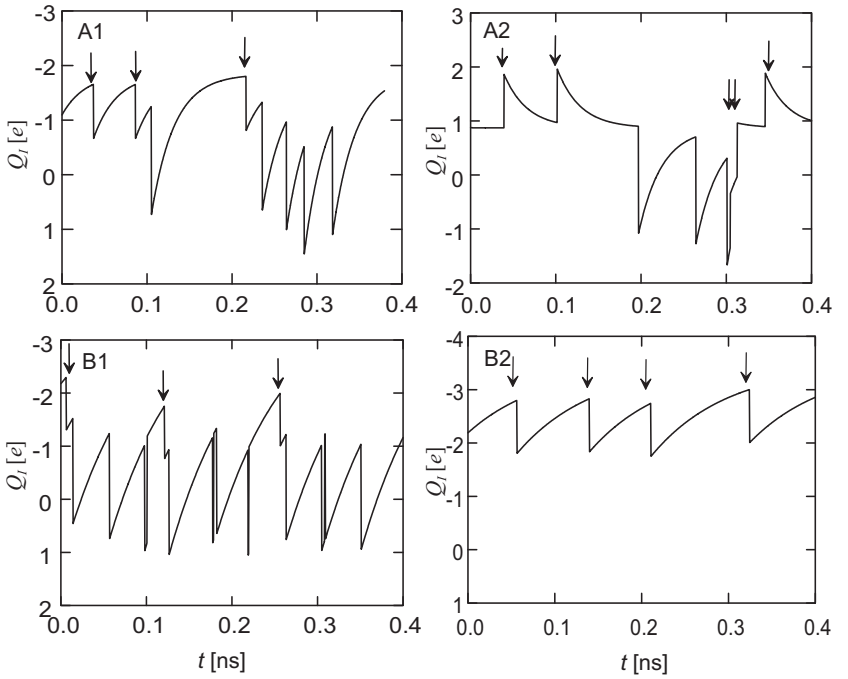

Figure 13. The island charge as function of time at different operating points for two different devices (see Fig. 12). Arrows mark quasiparticle tunneling events.

both branches. It is shown that at the upper branch there is a substantial Cooper pair current, whereas the lower branch consists of quasiparticle leakage only. In simulations the IV curves become more hysteretic as either Josephson coupling or the ratio of resistances R_c/R_{T1} is increased. The transition from hysteretic to nonhysteretic behavior is studied more quantitatively in the next section.

E. Analytic theory and noise properties

In this section we develop an analytic theory based on the assumption of the two-level system [11],[50]. At the first level the current through the JJ (the saturation current) is $I_S = 2ef_B$, where f_B is the frequency of Bloch oscillations. Therefore we may write the average collector current as

$$I_C = \frac{1/\Gamma_\uparrow}{1/\Gamma_\uparrow + 1/\Gamma_\downarrow} I_S - I_B, \tag{42}$$

where the prefactor of the first term is the share of time the system spends in the first level. The transition rates between the states are $\Gamma_\uparrow$ and $\Gamma_\downarrow$. The second term is the quasiparticle current from the base electrode, which leaks to the ground via the collector resistor. The base current is given as

$$I_B = -\frac{\langle N_e \rangle \, e}{1/\Gamma_\uparrow + 1/\Gamma_\downarrow}, \tag{43}$$

where $\langle N_e \rangle$ is the average number of electrons needed to cause a downwards transition. Here it is assumed that quasiparticles do not tunnel while the system is in the first level. If $\langle N_e \rangle$ differs from unity, it means that intralevel transitions are possible.

In Ref. P7 we give estimates for $\Gamma_\uparrow$, $\Gamma_\downarrow$, I_S, $\langle N \rangle$ and $\langle N_e \rangle$ in the limit of large resistance and low temperatures. Knowing them, it is possible to calculate IV curves of the BOT analytically. Comparisons to the simulations show reasonable agreement, though finite-temperature and impedance somewhat modify the properties. It is possible to calculate the small-signal response as well. It can be given by a conductance matrix

$$\begin{bmatrix} i_C \\ i_B \end{bmatrix} = \begin{bmatrix} G_{out} & g_m \\ g_x & G_{in} \end{bmatrix} \begin{bmatrix} v_C \\ v_B \end{bmatrix}, \tag{44}$$

where i_C, i_B, v_C and v_B are the small-signal components of collector and base currents and voltages, i.e. small variations around I_C, I_B, V_C and V_B. The small signal parameters are defined as $G_{out} = (\partial I_C/\partial V_C)_{V_B}$, $g_m = (\partial I_C/\partial V_B)_{V_C}$, $g_x = (\partial I_B/\partial V_C)_{V_B}$ and $G_{in} = (\partial I_B/\partial V_B)_{V_C}$.

It is possible to arrange the measurement so that V_C is kept constant at all times. This is the case for a small input impedance postamplifier, e.g. dc SQUID, whose inductive input impedance is close to zero at small frequencies. Even a large impedance of a voltage postamplifier can be dropped by applying current feedback. This renders output conductance G_{out} and intrinsic feedback transconductance g_x irrelevant. For this case the small signal model is graphically illustrated in the equivalent circuit of Fig. 14. The BOT is described with input impedance $R_{in} = 1/G_{in}$, and the current generator βi_B at the output driving the load resistance R_L, which is assumed small. The current gain is defined as

$$\beta = -\left(\frac{\partial I_C}{\partial I_B}\right)_{V_C} = -\frac{g_m}{G_{in}}. \tag{45}$$

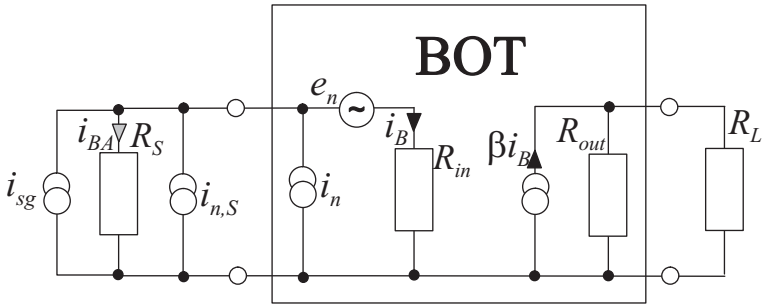

Figure 14. A small-signal model and equivalent noise sources of the BOT.

The signal source is described as Norton's equivalent, i.e. current generator i_{sg} in parallel with the source resistance R_S. The noise from the source is represented by generator $i_{n,S}$.

The noise added by the BOT is shown as equivalent voltage and current generators e_n and i_n, respectively, at the input. We assume that the dominant noise at the output is the two-level switching (telegraph) noise [51] inherent to the dynamics described above. In this case the equivalent sources can be shown to be fully correlated with spectral densities

$$S_{en}^{1/2} = \frac{2I_S}{-g_m}\sqrt{\frac{\Gamma_\downarrow\Gamma_\uparrow}{(\Gamma_\uparrow+\Gamma_\downarrow)^3}} \tag{46}$$

$$S_{in}^{1/2} = \frac{2I_S}{\beta}\sqrt{\frac{\Gamma_\downarrow\Gamma_\uparrow}{(\Gamma_\uparrow+\Gamma_\downarrow)^3}}. \tag{47}$$

This differs from the estimates given in Ref. P4, which assumes uncorrelated sources. However, it was later found that the correlations play a crucial role.

We next apply standard noise theory [52] to calculate the optimum noise resistance R_{opt} and minimum noise temperature T_n. Optimum noise resistance is the value of the source resistance R_S (see Fig. 14) with which the minimum noise temperature is obtained. These can be shown to be

$$R_{opt} = \sqrt{\frac{S_{en}}{S_{in}}} = R_{in} \tag{48}$$

$$T_n = \frac{1}{k_B}\sqrt{S_{en}S_{in}} = \frac{1}{k_B}R_{in}S_{in}. \tag{49}$$

In principle one can now calculate the small signal and noise parameters for a given device at a given bias point. This is, however, somewhat laborious, so in order to get an order of magnitude estimate and an idea about interdependencies, we next make some further simplifications. Two limits have to be considered separately, since for $V_C < 2V_Q \equiv 2e/C$ and $V_C > 2V_Q$ the dynamics is qualitatively different. In the first case $\langle N_e\rangle = 1$. In Ref. P7 we give approximations of some noise

properties. Here we further assume a typical point of operation ($V_C = (3/2)\,V_Q$ and $V_B = -V_Q$). It follows

$$\beta \approx 2\exp\left(\frac{\pi R e^2}{8\hbar}\left(\frac{E_J}{E_C}\right)^2\right) \tag{50}$$

$$g_m \approx -\frac{\beta}{R_T}\frac{1}{\left(1+(\ln 5)/4\,(R/R_T)\,\beta\right)^2} \tag{51}$$

$$S_{in}^{1/2} \approx \sqrt{\frac{4E_C}{R_T}\left(1+\frac{1}{4}\frac{R}{R_T}\ln(5)\,\beta\right)^{-3}} \tag{52}$$

$$S_{en}^{1/2} \approx \sqrt{4E_C R_T\left(1+\frac{\ln 5}{4}\left(\frac{R}{R_T}\right)\beta\right)} \tag{53}$$

$$R_{opt} \approx R_T\left(1+\frac{\ln 5}{4}\frac{R}{R_T}\beta\right)^2 \tag{54}$$

$$T_n \approx \frac{4E_C}{k_B}\left(1+\frac{\ln 5}{4}\frac{R}{R_T}\beta\right)^{-1}. \tag{55}$$

In this mode the BOT acts as a simple $e-2e\,\langle N\rangle$ -charge multiplier. Thus the current gain in Eq. (50) is actually $2\,\langle N\rangle$, i.e. the number of Cooper pairs in one "sequence" of Bloch oscillations. The current noise can also be given as $S_{in}^{1/2} = 2\sqrt{eI_B}\,(1+\Gamma_\downarrow/\Gamma_\uparrow)^{-1}$, i.e. it is essentially the shot noise of the input current times a suppression factor $(1+\Gamma_\downarrow/\Gamma_\uparrow)^{-1}$. A closer study of the dynamics shows that with large $\Gamma_\downarrow/\Gamma_\uparrow$ the noise at the output becomes fully anticorrelated with the noise at the input, which explains the reduction of the equivalent noise. Increasing the Josephson coupling E_J both increases the current gain and decreases the equivalent current noise and noise temperature. However, the transconductance gain drops and the optimum resistance increases simultaneously. The Josephson coupling cannot be increased beyond $E_J/E_C \approx 1$ for the assumptions of the model to hold. At finite temperature there will also be spontaneous downwards transitions due to incoherent Cooper pair tunneling which decreases the current gain [50]. This effect was excluded in this simplified model.

For $V_C > 2V_Q$ intralevel transitions become possible. This strongly modifies the dynamics yielding (see Ref. P7)

$$\beta \approx 1.2\,(1-\beta_B)^{-1} \tag{56}$$

$$g_m \approx -\frac{2}{R} \tag{57}$$

$$S_{in}^{1/2} \approx \frac{12e}{\sqrt{RC}}\left(\frac{R_T}{R}\right)\beta^{-1} \tag{58}$$

$$S_{en}^{1/2} \approx \frac{2e}{\sqrt{RC}}R_T \tag{59}$$

$$R_{opt} \approx \frac{R}{2}\beta \tag{60}$$

$$T_n \approx \frac{50E_C}{k_B}\left(\frac{R_T}{R}\right)^2\beta^{-1}. \tag{61}$$

This approximation is valid at $\beta_B \approx 1$. The hysteresis parameter of BOT, β_B, is defined as

$$\beta_B = -\frac{\Gamma_\downarrow (\Gamma_\uparrow + \Gamma_\downarrow)}{\Gamma_\uparrow \langle N_e \rangle} \left(\frac{\partial \langle N_e \rangle}{\partial V_B} / \frac{\partial \Gamma_\downarrow}{\partial V_B} \right), \tag{62}$$

and an estimate is given as

$$\beta_B \approx 0.02 \left(\frac{R}{R_T} \right)^2 \exp \left(\frac{\pi e^2 R}{16\hbar} \left(\frac{E_J}{E_c} \right)^2 \right). \tag{63}$$

The striking feature is the very strong dependence on β_B, which indicates that intraband transitions play an important role, since the sole effect of them was embedded in its definition (Eq. (62)). The value $\beta_B = 1$ leads to zero input conductance, which is due to the fact that changing V_B causes two competing effects. Firstly, it changes $\Gamma_\downarrow$, which leads to positive input conductance. Secondly, it changes $\langle N_e \rangle$, which leads to negative input conductance. If $\beta_B = 1$ these exactly cancel each other. This means that a small change in the input current causes a large change in the input voltage, and thus also the output current, and the current gain becomes large. Since the noise at the output remains finite, the effect also leads to decreasing equivalent noise.

The effect of increasing β_B is illustrated in the computed $I_C - I_B$ and $I_B - V_B$ plots in Fig. 15(a) and 15(b)). The Josephson coupling is varied. As β_B approaches unity the curves become hysteretic, indicating that the input conductance is negative. The increase of the gain and the

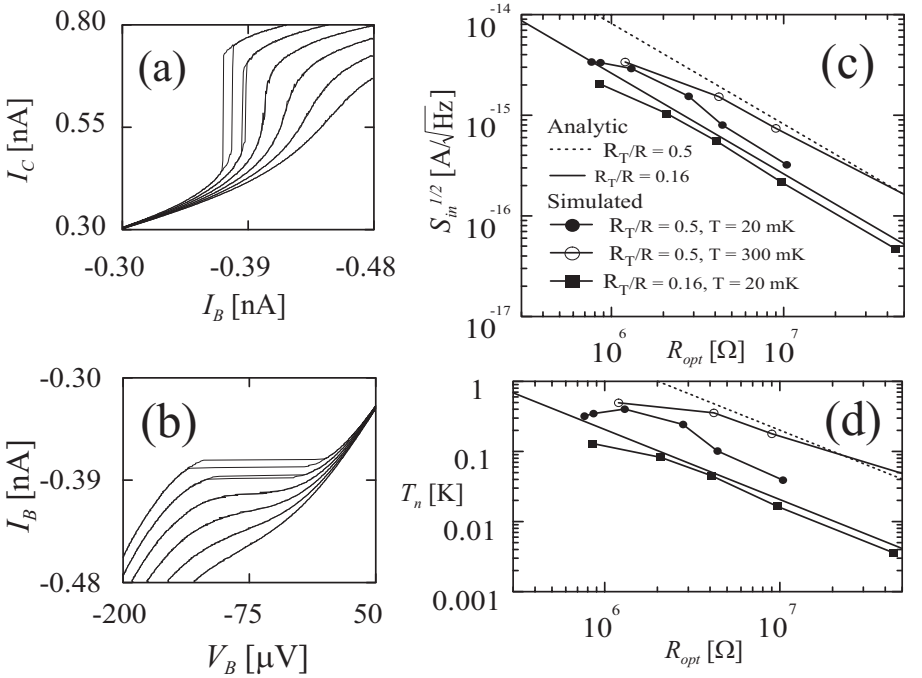

Figure 15. (a) and (b) Simulated characteristic curves with varying Josephson coupling. The base is current biased, so the negative input conductance appears as hysteresis. See Ref. P7 for the parameters used in the simulation. (c) and (d) The spectral current noise density and minimum noise temperature as function of the optimum noise resistance. Markers denote simulated and lines analytic results.

input impedance without a limit is also visible. In Fig. 15(c) and (d) equivalent current noise and noise temperature obtained from the simulations, together with the theoretical predictions from Eqs. (58), (60) and (61) are shown. Reasonable agreement is obtained despite the simplifying assumptions made along the derivation. This also indicates the improvement of noise properties as the optimum impedance increases. It suggests that BOT is a potential low noise amplifier for reading out sources with relatively large (of order 1 MΩ or more) impedances.

5. Summary

We have shown that the rich dynamics of Josephson junctions is of both theoretical and technological interest. Starting from the very basic description of a JJ, Eq. (1), we have derived models useful in realistic applications. The theoretical models were successfully tested in comparison with the experiments on the two devices under study. In both cases it was shown that the modelling techniques are sufficiently accurate for quantitative prediction of device properties as well as for optimizing them for practical purposes.

The new circuit solution for a programmable Josephson voltage standard was developed and optimized. Stable operation at about 1 V DC level with metrological accuracy was demonstrated experimentally. Characterization of the device together with preliminary experiments in AC generation suggest that it is also applicable in AC voltage metrology. A design with two independent outputs is potentially applicable in arbitrary impedance intercomparisons as well.

The principle of operation of the Bloch oscillating transistor was first demonstrated computationally. After the first experiments, the comparison to refined models showed that the device properties are quantitatively understood. Finally, an analytic theory was developed creating more tools for gaining insight into the device dynamics as well as for the device optimization. It was also shown that BOT can serve as a low-noise preamplifier in cryogenic circuits having an equivalent current noise spectral density below 1 $\mathrm{fA}/\sqrt{\mathrm{Hz}}$ and a noise temperature below 0.1 K.

References

[1] B.D. Josephson, Phys. Lett. 1, 251 (1962).

[2] T. van Duzer, Principles of Superconducting Devices and Circuits, Prentice Hall PTR, New Jersey (1999).

[3] K.K. Likharev, J. Low Temp. Phys. 59, 347 (1985).

[4] D.B. Haviland, L.S. Kuzmin, P. Delsing, and T. Claeson, Europhys. Lett. 16, 103 (1991).

[5] K.K Likharev, Dynamics of Josephson Junctions and Circuits, Gordon & Breach, New York (1986).

[6] R.L. Kauz, J. Appl. Phys. 58, 424 (1985).

[7] R.H. Koch, D.J. Van Harlingen, and J. Clarke, Phys. Rev. Lett. 45, 2132 (1980).

[8] J. Ziman, Principles of the Theory of Solids (Cambridge University Press, Campridge, 1972).

[9] U. Geigenmüller, and G. Schön, Phys. B 152, 186 (1988).

[10] G. Schön, and A.D. Zaikin, Phys. Rep. 198, 237 (1990).

[11] A.D. Zaikin, and D.S. Golubev, Phys. Lett. A 164, 337 (1992).

[12] A.O. Caldeira, and A.J. Legget, Phys. Rev. Lett. 46, 211 (1981).

[13] M.H. Devoret, D. Esteve, H. Grabert, G.-L. Ingold, H. Pothier, and C. Urbina, Phys. Rev. Lett. 64, 1824 (1990).

[14] G.-L. Inglold, and H. Grabert, Europhys. Lett. 14, 371 (1991).

[15] G.-L. Ingold, and Yu. V. Nazarov, in *Single Charge Tunneling*, eds. H. Grabert, and M.H. Devoret, Plenum Press, New York, pp. 21 - 107 (1992).

[16] R.L. Kauz, J. Appl. Phys. 52, 3528 (1981).

[17] R.L. Kauz, and R. Monaco, J. Appl. Phys. 57, 875 (1985).

[18] R.L. Kauz, J. Appl. Phys. 62, 424 (1987).

[19] R.L. Kauz, J. Appl. Phys. 76, 5538 (1994).

[20] S. Shapiro, Phys. Rev. Lett. 11, 80 (1963).

[21] W.H. Parker, B.N. Taylor, D.N. Langenberg, Phys. Rev. Lett. 18, 287 (1967).

[22] H. Seppä, P. Immonen, and J. Räihä, IEEE Trans. Instrum. Meas. 37, 2 (1988).

[23] F.L. Lloyd, C.A. Hamilton, J.A. Beall, D. Go, R.H. Ono, and R.E. Harris, IEEE Electron Dev. Lett. 8, 449 (1987).

[24] C.A. Hamilton, C. Burroughs, and K. Chieh, J. Res. Natl. Inst. Stand. Technol. 95, 219 (1990).

[25] R. Pöpel, Metrologia 29, 154 (1992).

[26] C.A. Hamilton, C. Burroughs, and R.L. Kautz, IEEE Trans. Instrum. Meas. 44, 223 (1995).

[27] S.P. Benz, C.A. Hamilton, C.J. Burroughs, and T.E. Harvey, Appl. Phys. Lett. 71, 1866 (1997).

[28] H. Schulze, F. Müller, R. Behr, J. Kohlmann, and J. Niemayer, and, D. Balashow, IEEE Trans. Appl. Supercond. 9, 4241 (1999).

[29] J. Kohlmann, F. Müller, P. Gutmann, R. Pöpel. L. Grimm, F.-W. Dünschende, W. Meier, and J. Niemeyer, IEEE Trans. Appl. Supercond. 7, 3411 (1997).

[30] T. Ryhänen, H. Seppä, R. Ilmoniemi, and J. Knuutila, J. Low Temp. Phys. 76, 287 (1989).

[31] L. Grönberg, H. Seppä, R. Cantor, M. Kiviranta, T. Ryhänen, J. Salmi, and I. Suni, Proceedings of the 4th International Conference SQUID'91, Berlin, 18 - 21 June 1991, 281 (1991).

[32] H. Seppä, M. Kiviranta, A. Satrapinski, L. Grönberg, J. Salmi and I. Suni, IEEE Trans. Appl. Supercond 3, 1816 (1993).

[33] H. Seppä, M. Kiviranta, and L. Grönberg, IEEE Trans. Appl. Supercond. 5, 3248 (1995).

[34] H. Seppä, M. Kiviranta, V. Virkki, L. Grönberg, J. Salonen, P. Majander, I. Suni, J. Simola, and A. Oittinen, Extended Abstracts of 6th International Superconductive Electronics Conference (ISEC'97), Braunschweig, Germany, 20 June 1997 (1997).

[35] M. Kiviranta, J.S. Penttilä, J. Hassel, A. Virtanen, and H. Seppä, Supercond. Sci. Technol. 17, 285 (2004).

[36] R. Behr, J. Kohlmann, J.-T.B.M Janssen, P. Kleinschmidt, J.M. Williams, S. Djordjevic, J.-P. Lo-Hive, F. Piquemal, P.-O. Hetland, D. Reymann, G. Eklund, C. Hof, C., B. Jeanneret, O. Chevtchenko, E. Houtzager, H.E. van den Brom, A. Sosso, D. Andreone, J. Nissila, and P. Helistö, IEEE Trans. Instrum. Meas. 52, 524 (2003).

[37] J. Hassel, P. Helistö, L. Grönberg, H. Seppä, J. Nissilä, and A. Kemppinen, "Stimulated Power Generation in es-SIS Junction Arrays", Submitted to IEEE Trans. Instrum. Meas.

[38] P. Helistö, J. Nissilä, K. Ojasalo, J.S. Penttilä, and H. Seppä, IEEE Trans. Instrum. Meas. 52, 533 (2003).

[39] J. Nissilä, K. Ojasalo, A. Kemppinen, A. Manninen, J. Hassel, P. Helistö, and H. Seppä, Conference of Precision Electromagnetic Measurement, London, 27. June - 2. July 2004, Conference Digest, 158 (2004).

[40] A. Kemppinen, Masters Thesis, Helsinki University of Technology (2004).

[41] D.V. Averin, and K.K. Likharev, J. Low Temp. Phys. 62, 345 (1986).

[42] D.V. Averin, and K. K. Likharev, in Mesoscopic Phenomena in Solids, eds. B.L. Altshuler, P.A. Lee, and R.A. Webb, Elsevier, Amsterdam, 173 (1991).

[43] T.A. Fulton, G.J. Dolan, Phys. Rev. Lett. 59, 109 (1987).

[44] A.N. Korotkov, and M. Paalanen, Appl. Phys. Lett. 74, 4052 (1999).

[45] A.B. Zorin, Phys. Rev. Lett. 76, 4408 (1996).

[46] R.J. Schoelkopf, P. Wahlgren, A.A. Kozhenikov, P. Delsing, and D.E. Prober, Science 280, 1238 (1998).

[47] M.A. Sillanpää, L. Roschier, and P. Hakonen, cond-mat/0402045 (2004).

[48] H. Seppä, Phys. B 284-288, 1804 (2000).

[49] A.N. Korotkov, Appl. Phys. Lett. 72, 3226 (1998).

[50] J. Delahaye, J. Hassel, R. Lindell, M. Sillanpää, M. Paalanen, H. Seppä, and P. Hakonen, Phys. E 18, 15 (2003).

[51] Sh. Kogan, Electronic Noise and Fluctuations in Solids, Cambridge University Press, Cambridge (1996).

[52] J. Engberg, and T. Larsen, Noise Theory of Linear and Nonlinear Circuits, John Wiley & Sons, New York (1995).

Errata

In the published versions of articles following misprints have been found.

P2

1. Section IIB: "$1/2\pi fC \gg 2\pi fL_J$" should be "$1/2\pi fC \ll 2\pi fL_J$".

2. Section IIB: "...transmission line inductance for the length of one junction is larger than the capacitive reactance, i.e. $s\ell_0 \gg 1/2\pi fC$, where ..."
should be
"...transmission line inductive reactance for the length of one junction is larger than the capacitive reactance, i.e. $2\pi fs\ell_0 \gg 1/2\pi fC$, where ...".

3. Section IIC: "...the initial and boundary conditions are $I(x,0) = 0$ for $0 < x < L$ and $I(0,t) = I(0,L) = I_0$."
should be
"...the initial and boundary conditions are $I(x,0) = 0$ for $0 < x < L$ and $I(0,t) = I(L,t) = I_0$."

4. Section IIC: Eq. (10) should stand

$$I(x,t) = I_0 \left(1 - \sum_{n=0}^{\infty} \frac{4}{(2n+1)\,\pi} \sin \frac{(2n+1)\,\pi x}{L} \exp\left(-(2n+1)^2 \frac{t}{\tau_{RC}}\right)\right)$$

5. SectionIID: In the last sentence ($j_c^{-4} f^{-1}$) should stand ($j_c^{-2} f^{-1}$).

P3

Eq. (1) should stand

$$\frac{\tau P^{1/2}}{(U\Delta I_n)^{5/2}} \propto f^{-5}$$

Published by

Series title, number and report code of publication

VTT Publications 551
VTT–PUBS–551

Author(s)
Hassel, Juha

Title

Josephson junctions in charge and phase picture
Theory and applications

Abstract

Properties of weak links between two superconductors, or Josephson junctions, make them interesting for fundamental physics research. Since their discovery over four decades ago, they have provided a unique way to study the behavior of the superconducting quantum phase. More recently, ultra small, or mesoscopic, Josephson junctions with substantial single Cooper pair charging energy have gained interest due to their behavior as macroscopic quantum objects.

In addition to the theoretical interest, Josephson junctions can be used as active elements in circuit applications. Particularly, in this Thesis we study two different devices. We develop the required theoretical treatments, derive device properties, and compare the results with experimental data.

The first application is a Josephson voltage standard based on externally damped Superconductor - Insulator - Superconductor junctions. It consists of an array of large Josephson junctions connected in series and irradiated with a 70 GHz microwave signal. Phase locking the Josephson dynamics into the signal leads to the quantization of the voltage. This is utilized in metrology. We introduce a new circuit solution based on frequency dependent damping of the junctions. Optimization and some designs for practical arrays are presented. The purpose is to find such a design that the array is fast, has low power consumption and is as stable as possible. Arrays able to generate DC voltages of order 1 volt with metrological accuracy are demonstrated experimentally and their applicability in AC voltage calibrations is analyzed.

The second application is the Bloch Oscillating Transistor (BOT). The BOT is based on controlling the Cooper pair current in an ultra small Josephson junction by means of quasiparticles tunneling through a normal junction. As part of the thesis work, the principle of operation is first demonstrated computationally. The model is then refined to yield quantitative predictions of the characteristics. Finally, an analytic theory for the device is developed and the properties as an amplifier are derived.

Keywords

Josephson junctions, quantum metrology, mesoscopic tunnel junctions

Activity unit

VTT Information Technology, Tietotie 3, P.O.Box 1207, FIN–02044 VTT, Finland

ISBN			Project number
951–38–6418–9 (soft back ed.) 951–38–6419–7 (URL:http://www.vtt.fi/inf/pdf/)			
Date October 2004	Language English	Pages 38 p. + app. 40 p.	Price B
Name of project		Commissioned by	
Series title and ISSN VTT Publications 1235–0621 (soft back ed.) 1455–0849 (URL: http://www.vtt.fi/inf/pdf/)		Sold by VTT Information Service P.O.Box 2000, FIN–02044 VTT, Finland Phone internat. +358 9 456 4404 Fax +358 9 456 4374	